Available online at www.sciencedirect.com
SCIENCE DIRECT®
European Journal of Mechanics A/Solids 25 (2006) 125–141

Compressive response of the Y-shaped sandwich core

C.B.W. Pedersen, V.S. Deshpande, N.A. Fleck *

Cambridge University Engineering Department, Trumpington Street, Cambridge, CB2 1PZ, UK

Received 28 January 2005; accepted 6 June 2005

Available online 16 September 2005

Abstract

The compressive response of the Y-shaped sandwich core has been investigated by analytical and finite element calculations. The effect of geometry, parent material properties and boundary conditions on the compressive response is explored in detail and models are developed for the stiffness, plastic collapse and elastic buckling strength of the Y-core. Practical Y-core geometries made from common structural alloys deform in an elastic-plastic manner; the elastic contribution to the collapse response can only be neglected for unrealistically low values of the parent material yield strain. Most practical Y-core designs have an almost constant collapse stress with increasing compressive strain implying that this geometry is an efficient energy absorbing structure.

Keywords: Sandwich structures; Effective properties; Elastic-plastic behaviour; Energy absorption; Y-core

1. Introduction

Commercial and military ship structures require adequate strength to survive impact by submerged rocks, icebergs and collisions with other vessels. Current designs are mainly based upon a monolithic skin with an internal stiffening and strengthening frame. Double-hulled designs have minimal coupling between the inner and outer hull. It is of current academic and industrial interest to determine whether significant enhancements in structural stiffness, strength, and energy absorption and a reduction in weight can be achieved by *sandwich construction*. Recently, a set of lattice materials have been devised for sandwich cores. These stretching-governed structures deform by axial extension of the constituent members with only a minor enhancement due to the bending stiffness of each member, see Deshpande et al. (2001). Consequently, they have a high specific stiffness and strength. These topologies include the pyramidal truss, the tetrahedral truss and the metal textile core, Wadley et al. (2004). In contrast, bending-governed micro-structures, such as metallic foams Ashby et al. (2000) and an egg-box material based upon a solid sheet or a wire mesh, have lower stiffness and strength than lattice materials (for a given relative density).

Weak sandwich cores of a ship hull can have an advantage over strong cores: they are able to diffuse an external transverse load over a wider area of hull without perforation, and reduce the propensity for shear-off of the sandwich panel from the supporting sub-structure. Recently, a Y-shaped sandwich core, manufactured by welding together steel sheets, has been proposed by Schelde Shipbuilding,[1] see Fig. 1. Full scale ship collision trials have confirmed the superior performance of such hull constructions with no tearing observed on either the outer or inner hull in the collision test; in contrast, the reference case of a

* Corresponding author. Fax: +44 1223 332662.
E-mail address: naf1@eng.cam.ac.uk.
[1] Royal Schelde, P.O. Box 16 4380 AA Vlissingen, The Netherlands.

0997-7538/$ – see front matter
doi:10.1016/j.euromechsol.2005.06.001

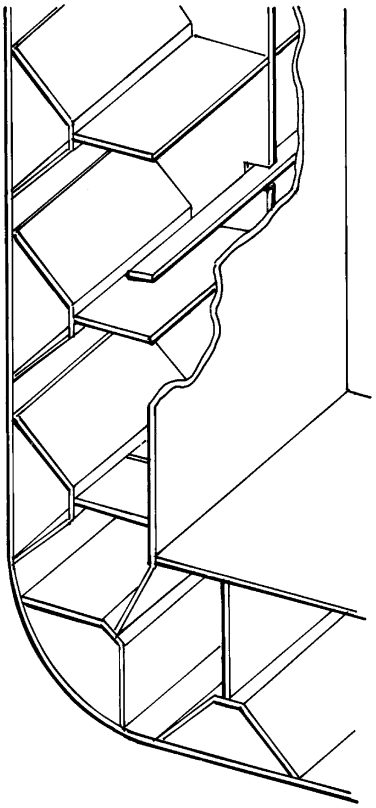

Fig. 1. Sketch of the Y-shaped sandwich core used in a sandwich hull ship construction.

single skin hull ruptured in an identical collision. It is argued that the ability of the bending-governed Y-core topology to spread the impact load over a wide area, combined with the high stretching resistance of the Y-core gives the enhanced performance.

1.1. Scope and limitations of the study

No detailed studies on the mechanics of the Y-core have been published to-date. Here we investigate the quasi-static compressive response of the Y-core between two rigid plates: this is representative of large body collisions in which a large number of the Y-supports are compressed simultaneously.

Here, we conduct a comprehensive theoretical investigation into the compressive response of the Y-core. Analytical and finite element predictions are made in order to understand the relation between the Y-core geometry and the macroscopic stiffness, strength and energy absorption capacity. The collapse modes include both elastic buckling and plastic yield, and the sensitivity of the compressive response to boundary conditions is investigated. It is shown that, practical Y-core geometries made from common structural alloys deform in an elastic-plastic manner. Thus, analytical calculations are unable to predict the compressive response and finite element calculations are required. The finite element calculations are used to produce maps of the compressive properties of the Y-core over a wide range of Y-core geometries and material properties.

2. Geometry of the Y-core

A unit cell of the Y-shaped sandwich core is sketched in Fig. 2. The geometry of the Y-core is described by the height h of the Y-core leg, the web size e, the inclination α of the Y-flanges, the thickness t of all the constituent members and the overall thickness H of the sandwich core. We define the non-dimensional leg height, web size and member thickness as

$$\bar{h} \equiv \frac{h}{H}, \quad \bar{e} \equiv \frac{e}{H} \quad \text{and} \quad \bar{t} \equiv \frac{t}{H}, \tag{1}$$

respectively.

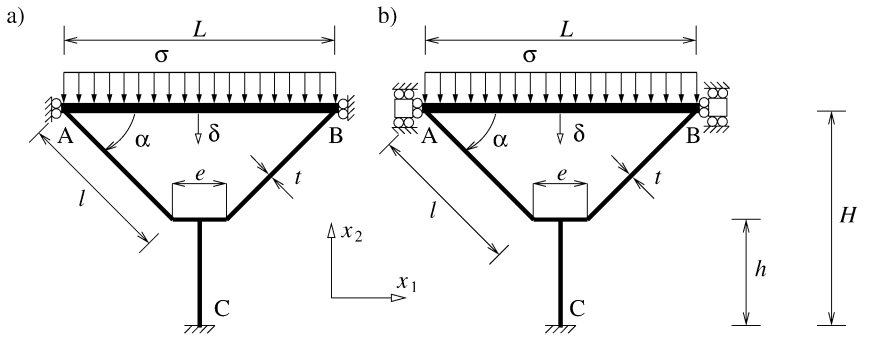

Fig. 2. Sketches of a unit cell of the Y-shaped sandwich core with the two types of boundary conditions analysed. (a) The no-sliding and (b) the free-sliding boundary condition. Note that the thicknesses of all members are equal to t.

Throughout this paper it is assumed that the unit cells are packed at the minimum spacing $L = e + 2(H - h)\cot\alpha$ such that adjacent Y-sections touch. The effective relative density of the Y-core (ratio of the density of the Y-core treated as a smeared-out continuum to the density of the solid material from which it is made) is given by

$$\bar{\rho} = \frac{2(1-\bar{h})\operatorname{cosec}\alpha + \bar{e} + \bar{h}}{2(1-\bar{h})\cot\alpha + \bar{e}}\bar{t}. \tag{2}$$

The compressive response of the Y-core is investigated for two choices of boundary conditions as sketched in Fig. 2:

1. *no-sliding*: The bottom of the Y-core is fully constrained, with the vertical and horizontal displacements $u_1 = 0$ and $u_2 = 0$, respectively. Further, the rotation $\theta = 0°$ at node C. At the top nodes A and B, the boundary conditions are $u_1 = 0$, $\theta = 0°$ and $u_2 = -\delta$, where δ is the applied compressive displacement;
2. *free-sliding*: The bottom of the Y-core is fully constrained, with $u_1 = u_2 = 0$ and $\theta = 0$. At the top nodes A and B, the rotation is $\theta = 0°$, the displacements u_1 are not constrained and the compressive displacement specified as $u_2 = -\delta$.

The above two sets of boundary conditions represent the limiting cases where the supports completely restrict and permit the sliding of the outer face of the ship hull with respect to the inner hull. Further, these two cases represent two typical experimental boundary conditions employed in laboratory scale investigations of the Y-core properties as in Rubino et al. (2005). It is worth mentioning that other boundary conditions which permit relative rotations of the two faces of the Y-core sandwich beams might also be relevant from a practical viewpoint but the two limiting cases described above are the most relevant for large structures comprising many Y-shaped webs.

3. Finite element study

We first report a set of finite element (FE) calculations to scope the competing mechanisms of compressive collapse of the Y-core. In these 2-dimensional FE calculations, the Y-core was modelled by 2D beam elements employing a co-rotational formulation, see Pedersen (2004) for details of the FE procedure. Typically, each constituent strut of the Y-core was discretised into 16 elements to capture the plastic buckling modes. Mesh sensitivity studies revealed that further mesh refinements does not improve accuracy appreciably. Unless otherwise stated, the Y-core was made from an elastic ideally-plastic solid with Young's Modulus $E_s = 210$ GPa, Poisson's ratio $\nu = 0.33$ and yield strength $\sigma_y = 300$ MPa giving a yield strain $\epsilon_y \equiv \sigma_y/E_s = 0.0014$. These values are representative of a structural steel.

The compressive behaviour of the Y-core was determined for the no-sliding and free-sliding boundary conditions sketched in Fig. 2. For both choices, the average compressive stress σ is defined as F/L, where F is the net force in the 2-direction at node C; the nominal compressive strain is given by $\epsilon \equiv \delta/H$.

We shall show below that the compressive response of the Y-core is strongly dependent upon the web dimension e. (In the current Schelde design[2] the web size is typically such that $\bar{e} = 0.1$.) In fact, the compressive response of the Y-core with no web ($e = 0$) is qualitatively different from the $e > 0$ case and we consider these cases separately. The $e = 0$ case shall be referred to as the "web-less Y-core" while the $e > 0$ case shall be referred to as the "regular Y-core".

[2] Private communication with Hans Ludolphe of Royal Schelde, The Netherlands.

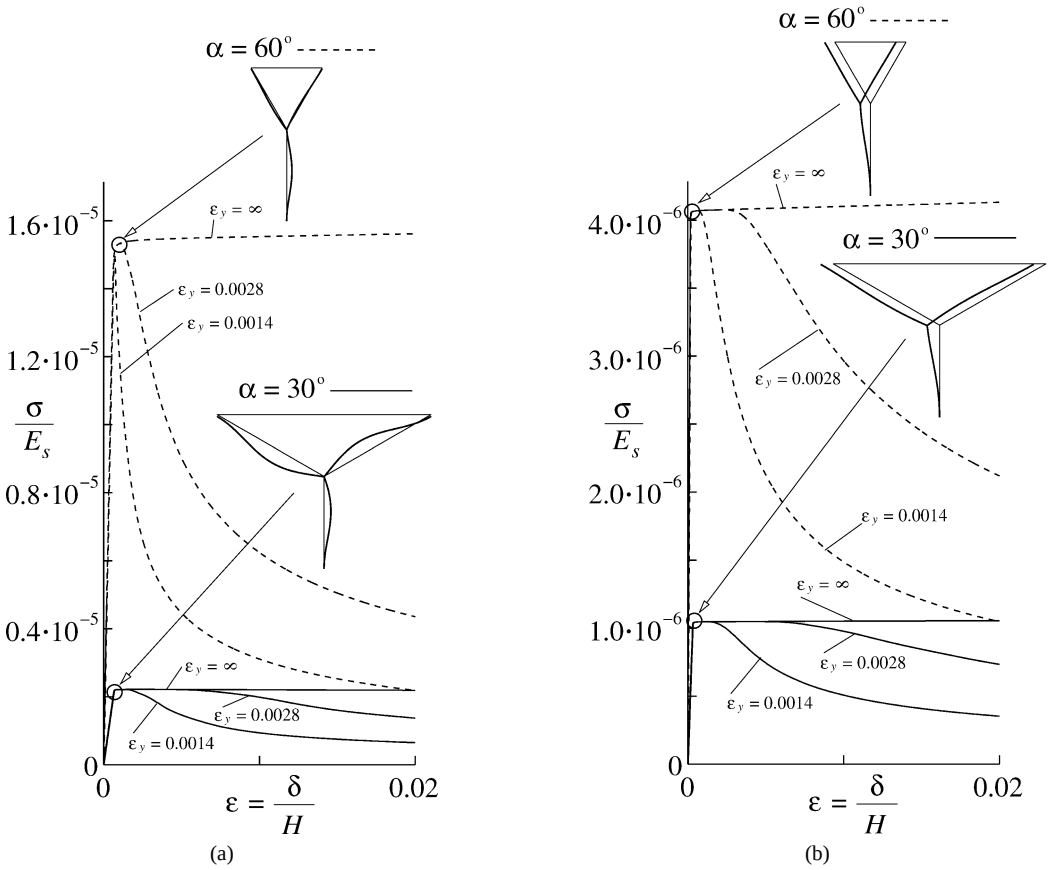

Fig. 3. Finite element predictions of the compressive stress versus strain curves of the web-less Y-core ($\bar{t} = 0.01$, $\bar{h} = 0.6$) for two choices of the Y-angle α. The FE predictions of the deformation modes in each case are also included. Results for both the (a) no-sliding and (b) free-sliding boundary conditions are shown.

3.1. Finite element modelling of the web-less Y-core ($e = 0$)

First consider Y-cores subjected to the no-sliding boundary condition and made from the reference material, $\epsilon_y = 0.0014$. The normalised stress, σ/E_s versus strain ϵ response of the Y-core ($\bar{t} = 0.01$ and $\bar{h} = 0.6$) is shown in Fig. 3(a) for two choices of the inclination $\alpha = 30°$ and $\alpha = 60°$. The $\alpha = 60°$ Y-core has a peak strength about five times greater than that of the $\alpha = 30°$ Y-core. The deformed FE meshes (displacements magnified by a factor of 3) at peak load are included in Fig. 3(a): while the $\alpha = 60°$ Y-core collapses by elastic buckling of the Y-core leg, the $\alpha = 30°$ Y-core buckles elastically in an unsymmetric mode with the inclined struts of the Y-arms buckling while the Y-core leg undergoes elastic bending. In the post-buckling regime rapid softening occurs due to plastic yield. In addition to the compressive stress versus strain curves of the Y-cores made from the reference material, $\epsilon_y = 0.0014$, the responses of Y-cores made from a material with a higher yield strain $\epsilon_y = 0.0028$ and for the elastic solid ($\epsilon_y = \infty$) are included in Fig. 3(a). In all cases, the normalised peak compressive strength p/E_s remains unchanged, confirming that the peak strength p is set by elastic buckling of the constituent struts. The post-peak softening behaviour is markedly reduced with increasing ϵ_y and is almost flat for $\epsilon_y = \infty$.

The stress versus strain curves of the above Y-cores with the free-sliding boundary condition are plotted Fig. 3(b). While the responses are qualitatively similar in shape to those with the no-sliding boundary condition, the peak strengths are about a factor of three smaller. This is rationalised by observing that the deformation modes of the Y-cores when sliding is permitted are different from the case when sliding is prohibited. Deformed FE meshes are included in Fig. 3(b) for the free sliding cases $\alpha = 30°$ and $\alpha = 60°$; the Y-cores collapse by elastic buckling of the Y-core legs, with the upper-half of the Y-core undergoing negligible deformation.

It is instructive to construct a collapse mechanism map for the web-less Y-core ($\bar{t} = 0.01, \epsilon_y = 0.0014$) with axes α and $\bar{h} \equiv h/H$, see Fig. 4(a). Contours of normalised peak compressive stress $p/(E_s\bar{\rho}^3)$ and relative density $\bar{\rho}$ are included in Fig. 4. This normalisation of the collapse stress is consistent with the fact that the elastic buckling stress scales with $\bar{\rho}^3 E_s$,

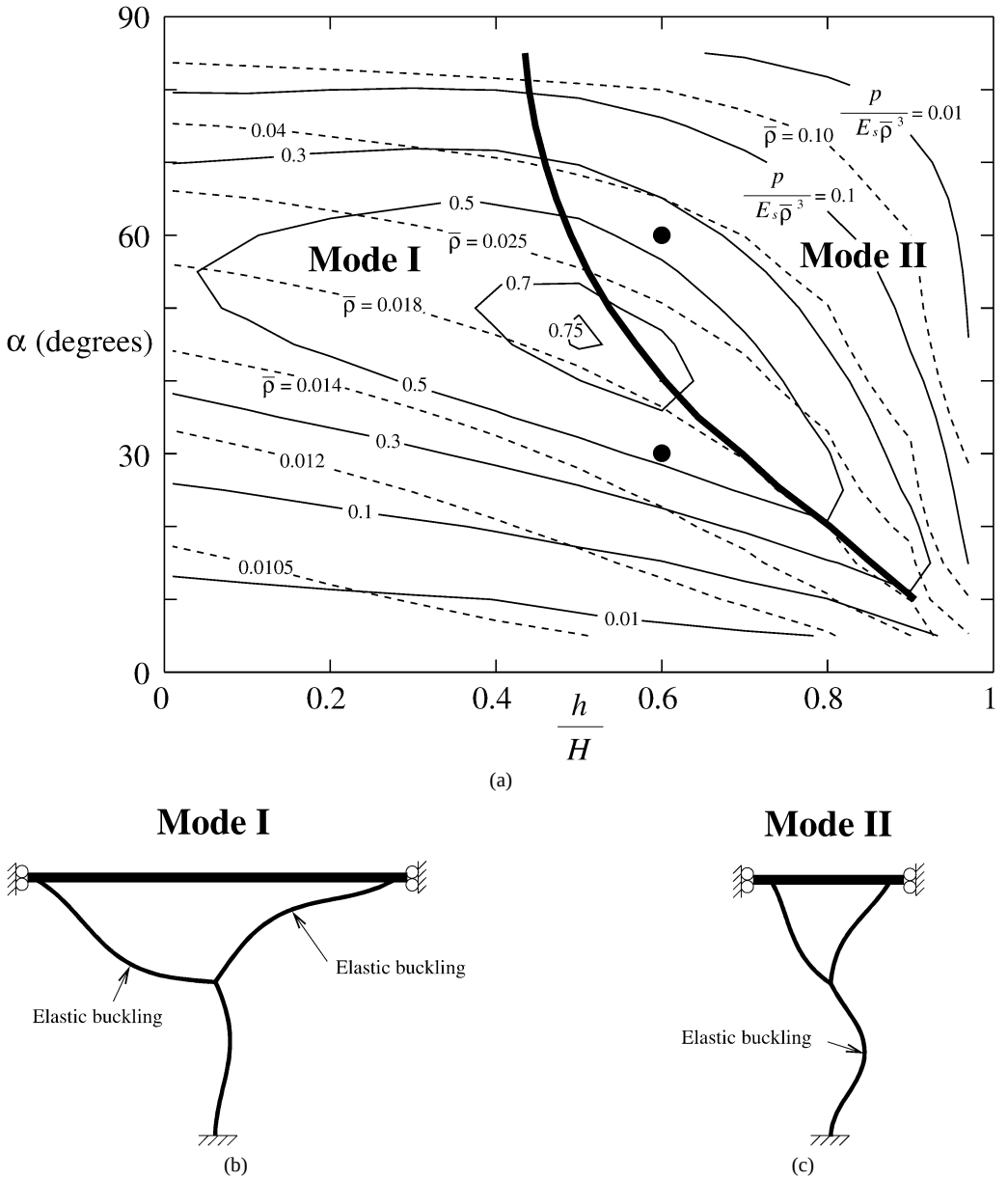

Fig. 4. (a) Collapse mechanism map of the web-less Y-core ($\bar{t} = 0.01$) with the no-sliding boundary condition. Contours of the normalised peak strength $p/(E_s\bar{\rho}^3)$ and relative density $\bar{\rho}$ are included and regimes of dominance of the two elastic buckling modes marked. Sketches of the (b) mode I and (c) mode II elastic buckling modes. The two data points marked correspond to the $\alpha = 30°$ and $\alpha = 60°$ Y-cores of Fig. 3.

see for example Gibson and Ashby (1997). The FE calculations reveal that the peak compressive stress p is dictated by elastic buckling over the entire map. Collapse is by one of the two possible elastic buckling modes I and II as sketched in Figs. 4(b) and 4(c). Analytical calculations of these two buckling modes are detailed in Section 4. The transition geometries for which collapse switches from one mode to the other is obtained by equating the analytical expressions for the two collapse loads; the resulting boundary of the collapse mechanism map is indicated by the thick solid line in Fig. 4(a). Consistent with the observations of the collapse modes in Fig. 3(a), the 30° Y-core with $\bar{h} = 0.6$ collapses in mode I while the 60° Y-core with $\bar{h} = 0.6$ collapses in mode II.

Finally, note that the stress versus strain response of the web-less Y-core is strongly softening for yield strains ϵ_y representative of most structural alloys. In energy absorption applications a flat collapse response is desirable and so the web-less Y-core is considered to be a poor choice.

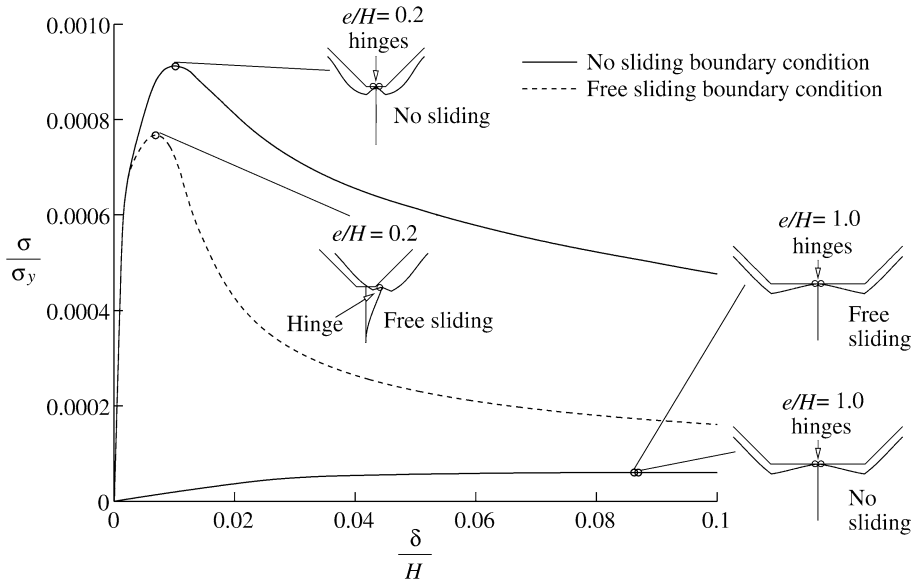

Fig. 5. Finite element predictions of the compressive stress versus strain response of the regular Y-core ($\alpha = 45°$, $\bar{t} = 0.01$, $\bar{h} = 0.6$) made from the reference material. Results are shown for two web sizes e and the two choices of boundary conditions. Deformed FE meshes showing the deformation modes in each case are also included.

3.2. Finite element modelling of the regular Y-core ($e > 0$)

3.2.1. No-sliding boundary condition

The compressive stress versus strain response of regular Y-cores ($\alpha = 45°$, $\bar{h} = 0.6$ and $\bar{t} = 0.01$) made from the reference material is shown in Fig. 5 for two choices of web size, $\bar{e} = 0.2$ and $\bar{e} = 1.0$. The $\bar{e} = 0.2$ Y-core has a softening post-peak compressive response. The $\bar{e} = 1.0$ Y-core is weaker but displays nearly no softening up to the strain levels computed here. Sketches of the deformation modes (displacements magnified by a factor of 6) are included in Fig. 5. The main deformation of both Y-cores occurs in the upper half of the Y-core with a plastic hinge forming at the mid-span of the web. While the inclined flanges of the $\bar{e} = 0.2$ Y-core undergo some elastic-plastic deformation the inclined flanges of the $\bar{e} = 1.0$ Y-core has plastic hinges at each end.

A collapse mechanism map for the regular Y-core ($\alpha = 45°$ and $\bar{t} = 0.01$) is shown in Fig. 6 with axes $\bar{e}$ and $\bar{h}$. Contours of the normalised peak compressive stress $p/(\sigma_y \bar{\rho}^2)$ and $\bar{\rho}$ are included in Fig. 6; the normalisation factor of $\bar{\rho}^2\sigma_y$ is consistent with the fact that the peak load is primarily governed by plastic bending, Gibson and Ashby (1997). When $\bar{e}$ or $\bar{h}$ are small, elastic buckling of the struts set the peak strength. Otherwise, peak load is dictated by the formation of plastic hinges as discussed above. These two regimes are marked in Fig. 6. Note that Y-cores with small webs are the most efficient from a strength perspective, giving the highest value of p for any $\bar{\rho}$. However, they collapse with a steeply dropping load, which is not efficient from an energy absorption standpoint.

The maps shown in Figs. 7 and 8 allow one to explore the sensitivity of p to α and $\bar{t}$. Comparing Figs. 7 ($\alpha = 30°$, $\bar{t} = 0.01$) and 8 ($\alpha = 45°$, $\bar{t} = 0.005$) with Fig. 6 indicates that elastic buckling is active for a larger fraction of the Y-core geometries when α or $\bar{t}$ is decreased. Additional numerical experimentation (and the analytical expressions of the following section) confirmed that the boundary between the elastic buckling and plastic bending regimes moves towards the upper right corner of the map with increasing ϵ_y.

Next, consider the energy absorption capability of the regular Y-core. We introduce the average collapse stress as

$$\overline{p} = \frac{\int_0^{\epsilon^*} \sigma \, \mathrm{d}\epsilon}{\epsilon^*}, \tag{3}$$

where ϵ^* is a permissible compressive strain in the core set by design considerations ($\bar{p}$ is a useful measure of energy absorption). In most energy absorption applications the aim is to absorb a given amount of energy with the peak stress p not exceeding a limiting value. Thus, an energy absorption efficiency measure is defined as $\eta \equiv \overline{p}/p$, with $\eta = 1$ representing an ideal energy absorber. An energy absorption map for the Y-core ($\alpha = 45°$ and $\bar{t} = 0.01$), with contours of $\overline{p}/p$ and $\bar{\rho}$, is plotted in Fig. 9 for

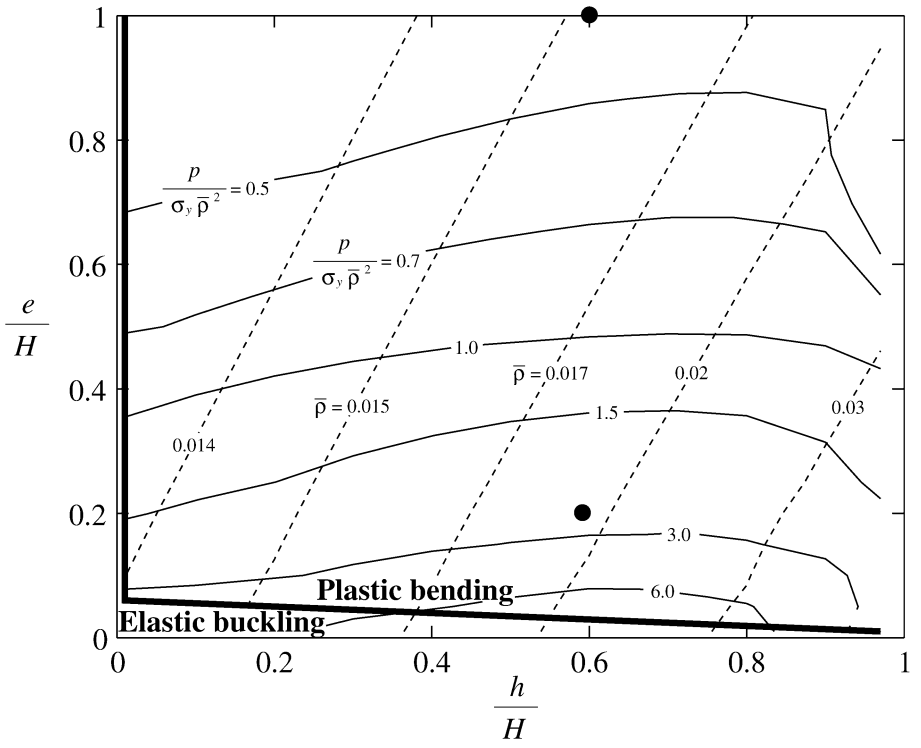

Fig. 6. Collapse mechanism map of the regular Y-core ($\alpha = 45°$, $\bar{t} = 0.01$) with the no-sliding boundary condition and made from the reference parent material. Contours of the normalised peak strength $p/(\sigma_y \bar{\rho}^2)$ and relative density $\bar{\rho}$ are included and regimes of dominance of the elastic buckling and plastic bending deformation modes are marked. The two data points marked correspond to the Y-cores of Fig. 5.

the choice $\epsilon^* = 0.1$. It is seen that Y-cores with large webs are the most efficient energy absorbers, although they possess a low peak collapse strength, cf. Fig. 6.

3.2.2. Free sliding boundary condition

The stress versus strain curves of the regular Y-cores ($\alpha = 45°$, $\bar{t} = 0.01$ and $\bar{h} = 0.6$) with sliding permitted are included in Fig. 5 for two choices of the web size $\bar{e}$. For $\bar{e} = 0.2$, both the peak strength and overall energy absorption capacity are lower than for the no-sliding case. On the other hand, for $\bar{e} = 1.0$, the stress versus strain responses of the Y-cores are nearly indistinguishable for the two different boundary conditions. The sketches of deformed Y-cores included in Fig. 5 reveal that the deformation mode is also insensitive to the choice of boundary condition for the choice $\bar{e} = 1.0$. In contrast, for the choice $\bar{e} = 0.2$, the single leg of the Y-core elastically buckles under free-sliding but undergoes nearly no deformation in the no-sliding case. We proceed to investigate the sensitivity of the peak strength and energy absorption capacity to the choice of boundary conditions.

Now consider the peak strength of the Y-cores made from the reference material with $\alpha = 45°$ and $\bar{t} = 0.01$. Define p_{fs} and p_{ns} as the peak strengths with free-sliding and no-sliding, respectively. The ratio p_{fs}/p_{ns} is plotted in Fig. 10 as a function of $\bar{h}$ for selected values of $\bar{e}$. For the web-less Y-core ($e = 0$), the ratio p_{fs}/p_{ns} decreases sharply with increasing $\bar{h}$. On the other hand, the $\bar{e} = 1.0$ Y-core is insensitive to the choice of boundary conditions and p_{fs}/p_{ns} equals unity for all values of $\bar{h}$ considered here. At intermediate values of $\bar{e}$ a transition in behaviour is observed with increasing $\bar{h}$: at low $\bar{h}$ we have $p_{fs}/p_{ns} = 1$ while above some critical value of $\bar{h}$, the ratio p_{fs}/p_{ns} drops with increasing $\bar{h}$.

Next, consider the influence of boundary condition upon the average collapse strength $\bar{p}$ for the choice $\epsilon^* = 0.1$. Define $\bar{p}_{fs}$ and $\bar{p}_{ns}$ as the average strengths with the free-sliding and no-sliding, respectively. The ratio $\bar{p}_{fs}/\bar{p}_{ns}$ is plotted as a function of $\bar{h}$ in Fig. 11 for selected values of $\bar{e}$. In similar manner to the peak strength, the average collapse strength of the web-less Y-core ($\bar{e} = 0$) is sensitive to the boundary conditions and $\bar{p}_{fs}/\bar{p}_{ns} < 1$ for all $\bar{h}$; in contrast, $\bar{p}_{fs}/\bar{p}_{ns} = 1$ when $\bar{e} = 1.0$. At intermediate values of $\bar{e}$, the ratio of the average collapse strengths becomes sensitive to the boundary conditions above a critical value of $\bar{h}$.

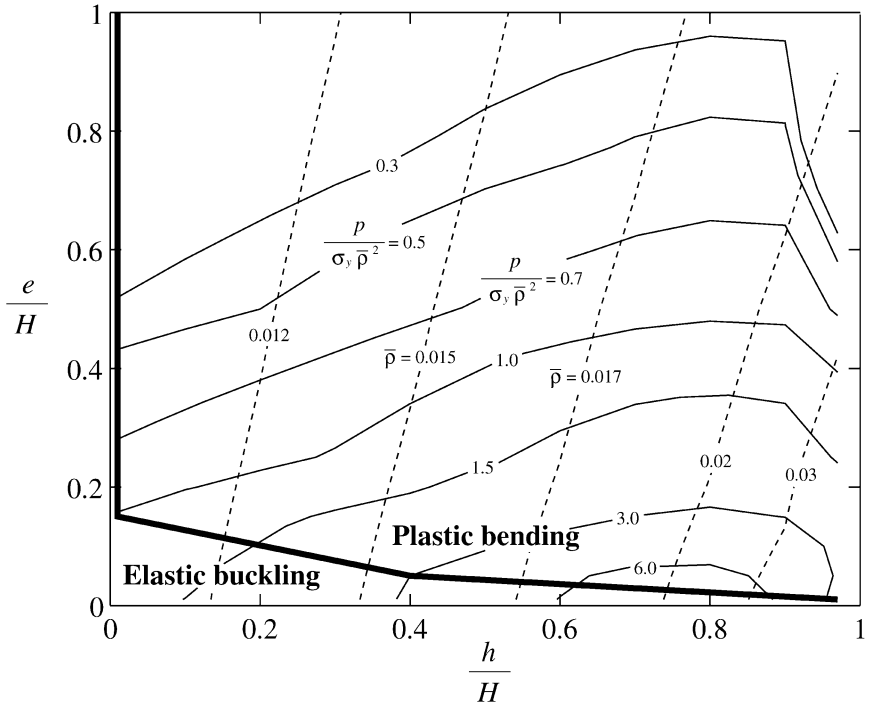

Fig. 7. Collapse mechanism map of the regular Y-core ($\alpha = 30°$, $\bar{t} = 0.01$) with the no-sliding boundary condition and made from the reference parent material. Contours of the normalised peak strength $p/(\sigma_y \bar{\rho}^2)$ and relative density $\bar{\rho}$ are included and regimes of dominance of the elastic buckling and plastic bending deformation modes are marked.

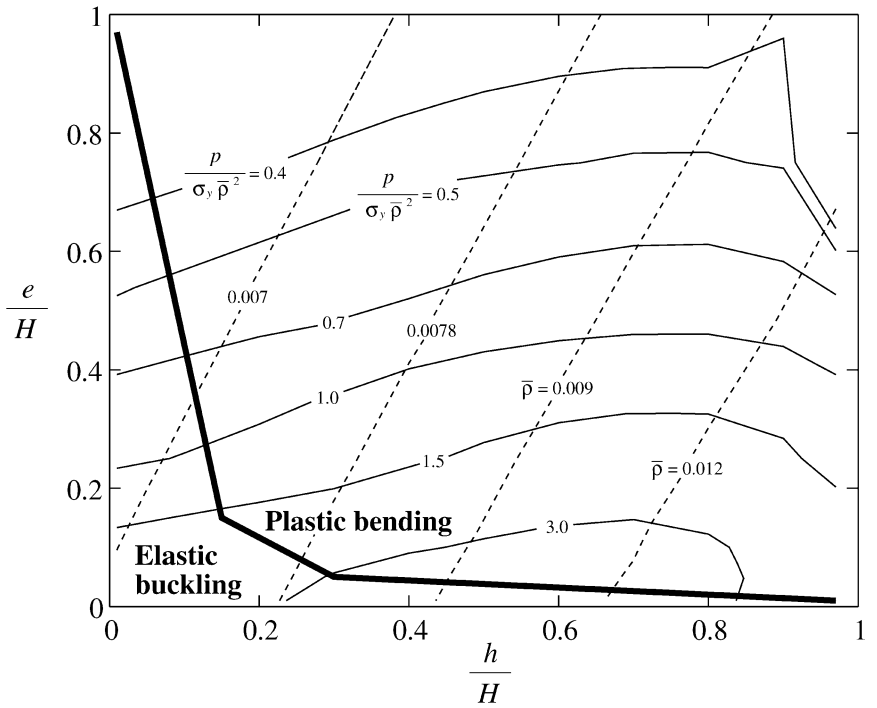

Fig. 8. Collapse mechanism map of the regular Y-core ($\alpha = 45°$, $\bar{t} = 0.005$) with the no-sliding boundary condition and made from the reference parent material. Contours of the normalised peak strength $p/(\sigma_y \bar{\rho}^2)$ and relative density $\bar{\rho}$ are included and regimes of dominance of the elastic buckling and plastic bending deformation modes are marked.

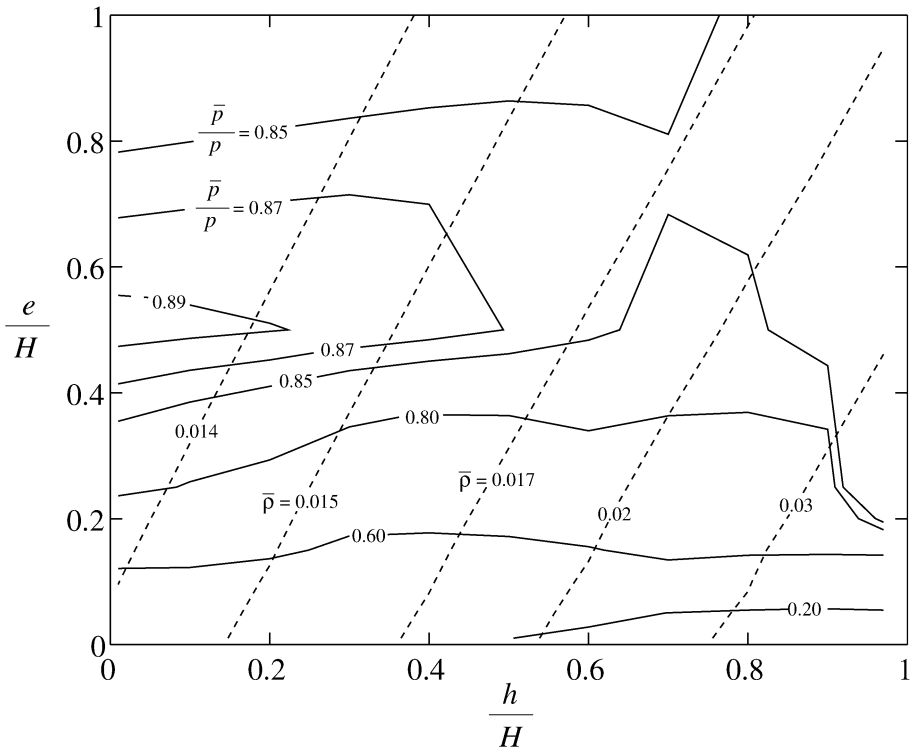

Fig. 9. Average collapse strength map of the regular Y-core ($\alpha = 45°$, $\bar{t} = 0.01$) with the no-sliding boundary condition and made from the reference parent material. Contours of the normalised energy absorption capacity $\bar{p}/p$ ($\epsilon^* = 0.1$) and relative density $\bar{\rho}$ are included.

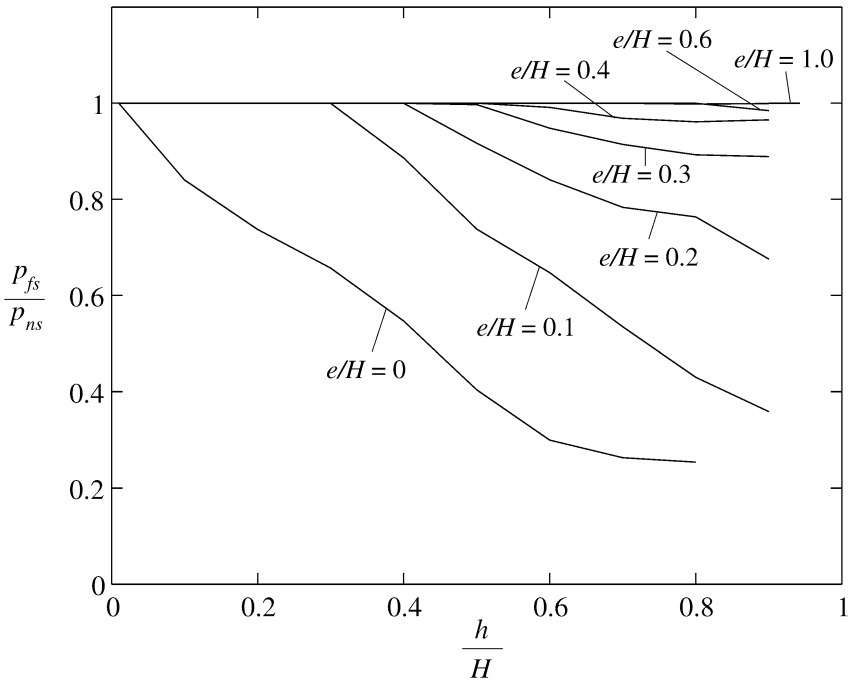

Fig. 10. Ratio of the peak compressive strengths p_{fs}/p_{ns} of Y-cores compressed with the free sliding and no sliding boundary conditions as the function of the leg height $\bar{h}$. The FE results are shown for Y-cores ($\alpha = 45°$, $\bar{t} = 0.01$) made from the reference parent material for selected web sizes $\bar{e}$.

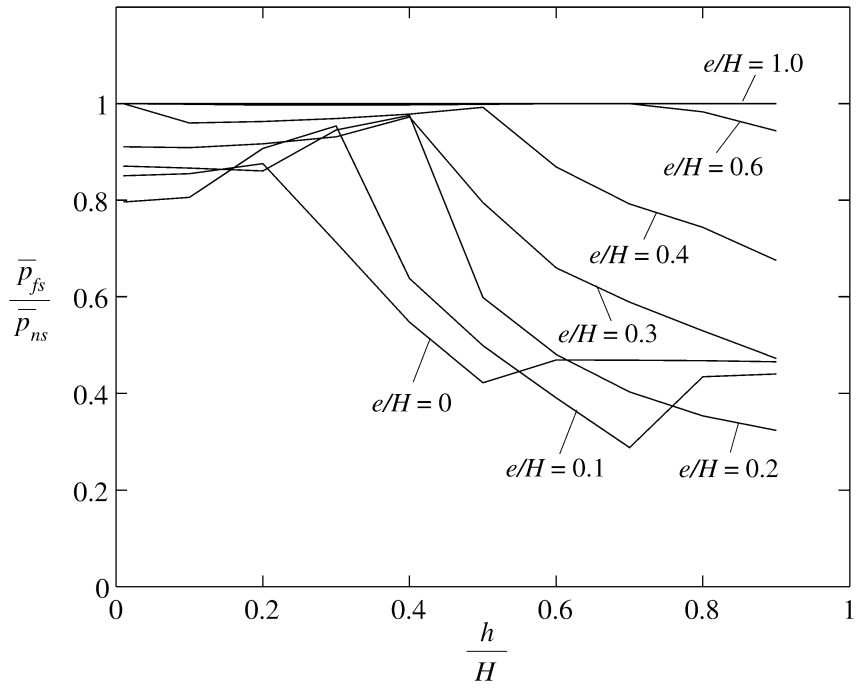

Fig. 11. Ratio of the average collapse strengths $\bar{p}_{fs}/\bar{p}_{ns}$ (at $\epsilon^* = 0.1$) of Y-cores compressed with the free sliding and no sliding boundary conditions as the function of the leg height $\bar{h}$. The FE results are shown for Y-cores ($\alpha = 45°$, $\bar{t} = 0.01$) made from the reference parent material for selected web sizes $\bar{e}$.

4. Analytical predictions of the stiffness and collapse strength

Motivated by the finite element calculations detailed above, we now present analytical models for the elastic stiffness and strength of both the web-less and regular Y-cores. The elastic buckling calculations assume no-sliding, while the plastic collapse calculations hold for both boundary conditions. This section concludes with a comparison of the analytical and FE predictions.

4.1. Web-less Y-core ($e = 0$)

4.1.1. Elastic stiffness

For small values of t/L, the contribution to the overall stiffness from bending of the constituent members of the web-less Y-core is small. Thus, the Y-core members may be assumed to be pin-jointed and the Young's modulus E of the Y-core is then given by simple truss theory as

$$\frac{E}{E_s} = \frac{\tan\alpha \sin^3\alpha}{(1-\bar{h})[(1-\bar{h}) + 2\bar{h}\sin^3\alpha]}\bar{t}, \tag{4}$$

where E_s is the Young's modulus of the parent material.

4.1.2. Elastic buckling

The FE calculations presented in Section 3 suggest two possible elastic buckling modes for the web-less Y-core. We now analyse these modes for a Y-core made from a parent material with Young's modulus E_s.

Mode I: This mode involves elastic buckling of the inclined struts with the Y-core leg acting as a rotational elastic spring, see Fig. 4(b). The buckling load for each inclined strut in the upper-half of the Y-core can be estimated by analysing the buckling of the column sketched in Fig. 12(a). The rotational spring represents the constraint exerted by the Y-core leg, with a stiffness $K_\theta = E_s t^3/6h$ per unit depth. Employing the analysis of Timoshenko and Gere (1963), the elastic buckling stress p of the Y-core in mode I is given by the implicit relation

$$\psi(u)\left[6\frac{h}{l} + 4\psi(u)\right] - \left[\phi(u)\right]^2 = 0, \tag{5a}$$

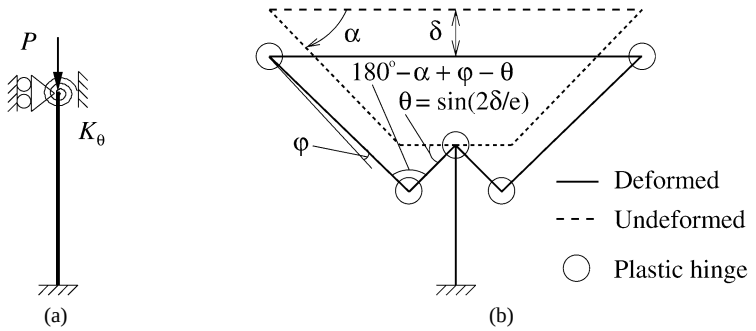

Fig. 12. (a) Sketch of the column clamped at one end and constrained against rotation by a spring of stiffness K_θ at the other end. (b) Collapse mechanisms of the regular Y-core employed in the rigid ideally-plastic analysis.

where

$$u = \frac{l}{2t}\sqrt{\frac{6pL}{\sin\alpha E_s t}} \tag{5b}$$

and

$$\phi(u) = \frac{3}{u}\left(\frac{1}{\sin(2u)} - \frac{1}{2u}\right) \quad \text{and} \quad \psi(u) = \frac{3}{2u}\left(\frac{1}{2u} + \frac{1}{\tan(2u)}\right). \tag{6}$$

Recall that $l \equiv (H-h)/\sin\alpha$ and $L \equiv e + 2(H-h)\cot\alpha$ denote geometric parameters of the Y-core as sketched in Fig. 2.

Mode II: The leg of the Y-core buckles elastically while the inclined struts in the upper half bend elastically and provide rotational constraint (Fig. 4(c)). Thus, the buckling load of the Y-core leg can be estimated by analysing the buckling of the column as sketched in Fig. 12(a), with $K_\theta = 2E_s t^3/3l$, per unit depth. The mode II elastic buckling stress p of the Y-core is given by

$$\psi(u)\left[\frac{3l}{2h} + 4\psi(u)\right] - \left[\phi(u)\right]^2 = 0 \quad \text{where } u = \frac{h}{2t}\sqrt{\frac{12pL}{E_s t}}, \tag{7}$$

where $\phi(u)$ and $\psi(u)$ are defined in (6).

The elastic buckling strength p for a given Y-core geometry is determined by the lower collapse strength of (5b) and (7). This analysis is in excellent agreement with the FE results of Section 3.1 and thus explicit comparisons are omitted for the sake of brevity. Note that this analysis is used to define the transition line between the two collapse modes in the map in Fig. 4.

4.1.3. Plastic collapse strength

Next, consider a web-less Y-core made from a rigid, ideally plastic parent material of yield strength σ_y. Plastic collapse of the Y-core can occur by two possible modes (i) axial yielding of the Y-core leg with the upper-half remaining rigid and (ii) axial yielding of the struts in the upper-half of the Y-core with the leg remaining rigid. Equilibrium considerations give the plastic collapse strength p directly as

$$\frac{p}{\sigma_y} = \begin{cases} \dfrac{t}{L} = \dfrac{1}{2(1-\bar{h})\cot\alpha}\,\bar{t} & \text{if } \alpha > 30^\circ, \\ 2\sin\alpha\,\dfrac{t}{L} = \dfrac{\cos\alpha}{1-\bar{h}}\,\bar{t} & \text{otherwise.} \end{cases} \tag{8}$$

The operative collapse mode is the one associated with the lower collapse load and so mode (i) is operative for $\alpha > 30^\circ$ while mode (ii) is active for $\alpha \leqslant 30^\circ$. It is emphasised that for a parent material yield strain ϵ_y representative of most common structural alloys, the plastic collapse strengths given by (8) are much higher than the elastic buckling strengths for any realistic Y-core design. Hence, for the reference case, $\epsilon_y = 0.0014$, the plastic yielding mode is never operative for the web-less Y-core, recall Fig. 4.

4.2. Regular Y-core

The finite element calculations presented in Section 3 revealed that the peak strength of the regular Y-core ($e > 0$) is generally governed by plastic collapse. The exception is for a very small web size e; then, elastic buckling dominates and the analytical

elastic buckling analysis of the web-less Y-core is applicable. We proceed to present analytical formulae for only the elastic stiffness, plastic collapse strength and energy absorption capacity of the regular Y-core.

4.2.1. Elastic stiffness

The overall compliance of the Y-core can be calculated as the sum of the contributions from bending and of stretching of the struts. In the absence of stretching, bending of the horizontal and inclined struts of the upper half of the Y-core gives an effective Young's modulus E of the Y-core as

$$\frac{E_{\text{bending}}}{E_s} = \frac{8}{\bar{e} + 2(1-\bar{h})\cot\alpha}\left(\frac{\bar{t}}{\bar{e}}\right)^3 \frac{2\bar{e}\sin\alpha + (1-\bar{h})}{\bar{e}\sin\alpha + 2(1-\bar{h})}. \tag{9}$$

Alternatively, the stiffness $E_{\text{stretching}}$ associated with axial stretching of the struts is given by (4). Hence, the effective Young's modulus of the Y-core, due to both the bending and stretching contributions follows by linear summation of the compliances as

$$\frac{1}{E} = \frac{1}{E_{\text{bending}}} + \frac{1}{E_{\text{stretching}}}. \tag{10}$$

4.2.2. Plastic collapse strength and energy absorption

The plastic collapse mode for a regular Y-core made from a rigid, ideally plastic parent material is sketched in Fig. 12(b). The collapse mode involves rotation about the five plastic hinges sketched in Fig. 12(b) with no axial stretching of any of the Y-core struts. For a given compressive displacement δ, the plastic dissipation U per unit depth due to relative rotations at the plastic hinges is given by

$$U = 2M_p\left[\varphi + (180^\circ - \alpha) - (180^\circ - \alpha + \varphi - \theta) + \theta\right] = \sigma_y t^2 \sin^{-1}\left(\frac{2\delta}{e}\right), \tag{11}$$

where the angles φ, θ and α are defined in Fig. 12(b) and $M_p = \sigma_y t^2/4$ is the plastic moment per unit depth of the Y-core struts. Equating the internal plastic dissipation U to the external work $L\int_0^\delta \sigma\,\mathrm{d}\delta$, gives an analytical expression for the stress σ versus strain $\epsilon \equiv \delta/H$ response of the Y-core as

$$\frac{\sigma}{\sigma_y} = 2\left(\frac{\bar{t}}{\bar{e}}\right)\frac{\bar{t}}{\bar{e} + 2(1-\bar{h})\cot\alpha}\frac{1}{\sqrt{1-(2\epsilon/\bar{e})^2}}, \tag{12}$$

and thus the initial collapse strength

$$\frac{p(\delta=0)}{\sigma_y} = 2\left(\frac{\bar{t}}{\bar{e}}\right)\frac{\bar{t}}{\bar{e} + 2(1-\bar{h})\cot\alpha}. \tag{13}$$

The average collapse strength $\bar{p}$ of the Y-core is

$$\frac{\bar{p}}{\sigma_y} = \frac{U}{\epsilon^* LH\sigma_y} = \frac{\bar{t}^2}{\epsilon^*[\bar{e} + 2(1-\bar{h})\cot\alpha]}\sin^{-1}\left(\frac{2\epsilon^*}{\bar{e}}\right), \tag{14}$$

up to any strain level ϵ^*. Note that this simple model ignores any deformations in the leg of the Y-core and predicts a hardening compressive stress versus strain response of the Y-core while the FE calculations shown in Fig. 5 predict a softening response. This discrepancy is due to the neglect of elasticity in the rigid, ideally plastic analysis: elastic deformations are significant for the case in $\epsilon_y = 0.0014$ as shown in Fig. 5.

4.3. Comparison of finite element and analytical predictions

Comparisons of the FE and analytical predictions of the Young's modulus E for Y-cores ($\alpha = 45^\circ$, $\bar{t} = 0.01$ and $\bar{e} = 0.2$) are shown in Fig. 13(a) as a function of the leg height $\bar{h}$. The small web size leads to small bending moments and small bending deflections of the Y-core. Consequently, both the FE and analytical predictions of the normalised stiffness $E/(E_s/\bar{\rho}^3)$ much exceed unity. The FE predictions agree well with the analytical model when both stretching and bending deformations are considered, Eq. (10). Comparisons of the analytical and FE predictions of the initial collapse strength p are shown in Fig. 13(b) for Y-cores made from the reference material ($\epsilon_y = 0.0014$). The analytical model substantially over-predicts p for the practical range of leg heights $\bar{h} < 0.3$. FE predictions of $\bar{p}$ for the choice $\epsilon^* = 0.1$ are included in Fig. 13(b). Again, the analytical model substantially over-predicts $\bar{p}$.

Next consider the Y-core with a large web $\bar{e} = 1.0$. Comparisons of the analytical and FE predictions for this Y-core ($\bar{e} = 1.0$, $\alpha = 45^\circ$ and $\bar{t} = 0.01$) are given in Fig. 14. With this large web, the stiffness of the Y-core is bending governed with $E/(E_s\bar{\rho}^3) \approx 1$ (Fig. 14(a)). This dependence upon $\bar{\rho}$ mimics the in-plane response of hexagonal honeycombs Gibson and

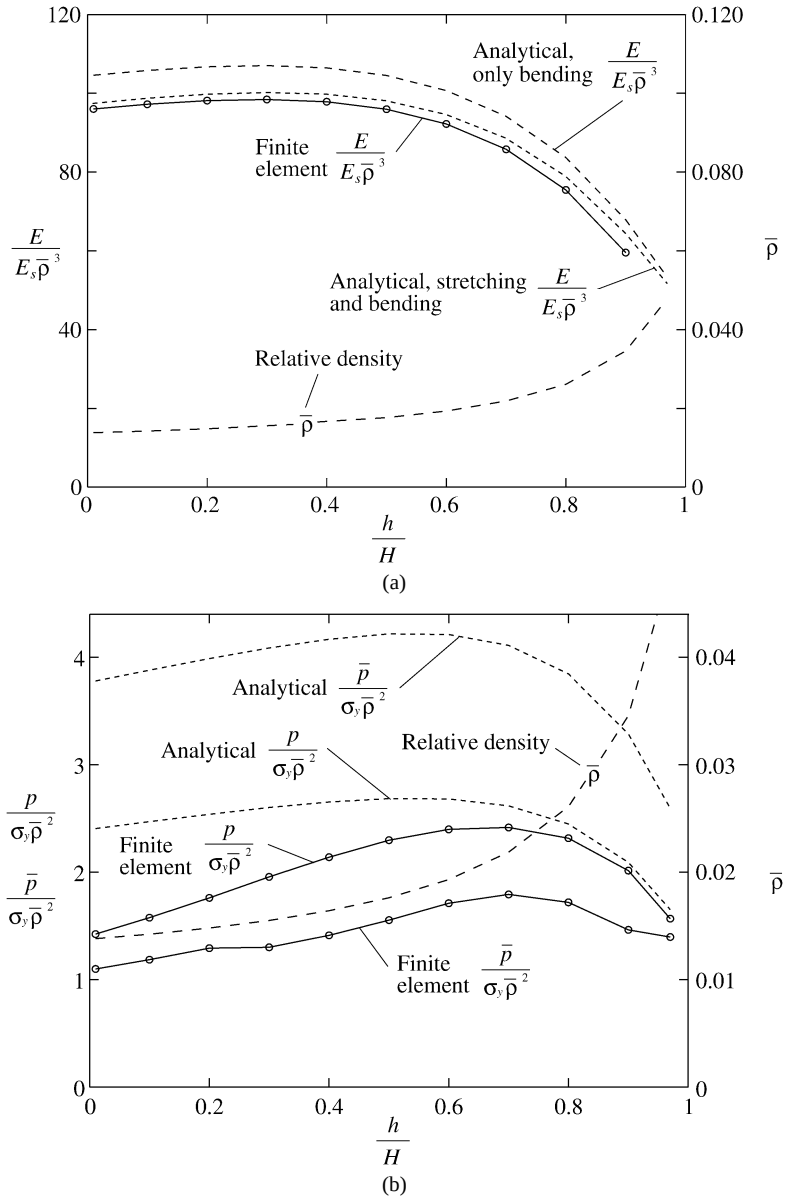

Fig. 13. Comparison between analytical and FE predictions of (a) the Young's modulus E and (b) peak collapse strength p and average collapse strength $\bar{p}$ (at $\epsilon^* = 0.1$) of regular Y-cores ($\alpha = 45°$, $\bar{t} = 0.01$, $\bar{e} = 0.2$) made from the reference parent material. All calculations pertain to the no-sliding boundary condition.

Ashby (1997). Thus, the analytical predictions (4) and (10) are approximately equal and agree well with the FE calculations. Similar to the Y-core with $\bar{e} = 0.2$, the analytical model substantially over-predicts both p and $\bar{p}$ (at $\epsilon^* = 0.1$) for Y-cores made from the reference material properties (Fig. 14(b)).

4.4. Effect of the yield strain ϵ_y on the collapse strength

Recall that elastic buckling is not operative for the Y-cores in Figs. 13 and 14. Consequently, the discrepancies between the rigid, ideally plastic analytical calculations and the FE calculations are likely to be a result of elastic-plastic deformations of the Y-core. In order to investigate the effect of elastic-plastic deformations on the collapse strength of the Y-core we explore the effect of the yield strain ϵ_y of the parent material upon the collapse strength p with the no-sliding boundary condition: the analytical predictions of the collapse strength p should agree with the FE calculations in the limit $\epsilon_y \to 0$.

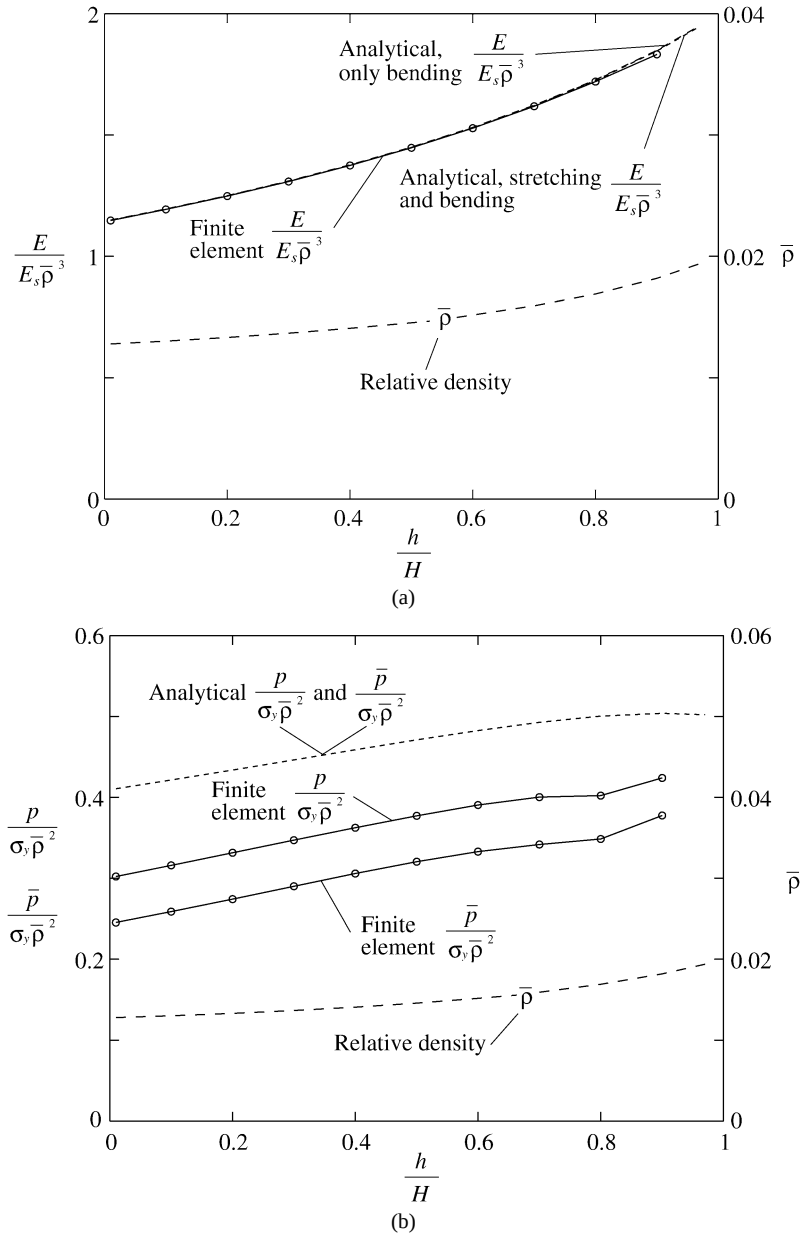

Fig. 14. Comparison between analytical and FE predictions of (a) the Young's modulus E and (b) peak collapse strength p and average collapse strength $\bar{p}$ (at $\epsilon^* = 0.1$) of regular Y-cores ($\alpha = 45°$, $\bar{t} = 0.01$, $\bar{e} = 1.0$) made from the reference parent material. All calculations pertain to the no-sliding boundary condition.

FE calculations of the peak collapse strength p of the Y-core are plotted against ϵ_y in Fig. 15 for the choice $\bar{e} = 0.2$, and in Fig. 16 for a larger web $\bar{e} = 1.0$. In both figures the geometry is specified by $\alpha = 45°$, $\bar{t} = 0.01$, $\bar{h} = 0.2$ and 0.6. FE predictions of the elastic buckling stresses and rigid, ideally plastic analytical estimates of the collapse strength are included in both figures. For both web sizes, the FE predictions of p agree well with the rigid, ideally plastic analytical predictions for $\epsilon_y < 10^{-4}$ while at large values of ϵ_y, p is governed by elastic buckling (the FE calculations shown here over-predict the collapse strength p in the limit $\epsilon_y \to 0$. This is due to mesh resolution issues: spot calculations with a much finer mesh revealed near perfect agreement between the FE and analytical calculations). Structural alloys possess a yield strain in the range of 0.001 to 0.01, with a representative value given by that of the reference material, $\epsilon_y = 0.0014$. For yield strains in this range, Y-cores lie in the transition between elastic buckling and plastic collapse. We conclude that neither the elastic buckling formulae nor the rigid-plastic collapse formulae of Section 4 can be used in a conservative manner for practical Y-core designs.

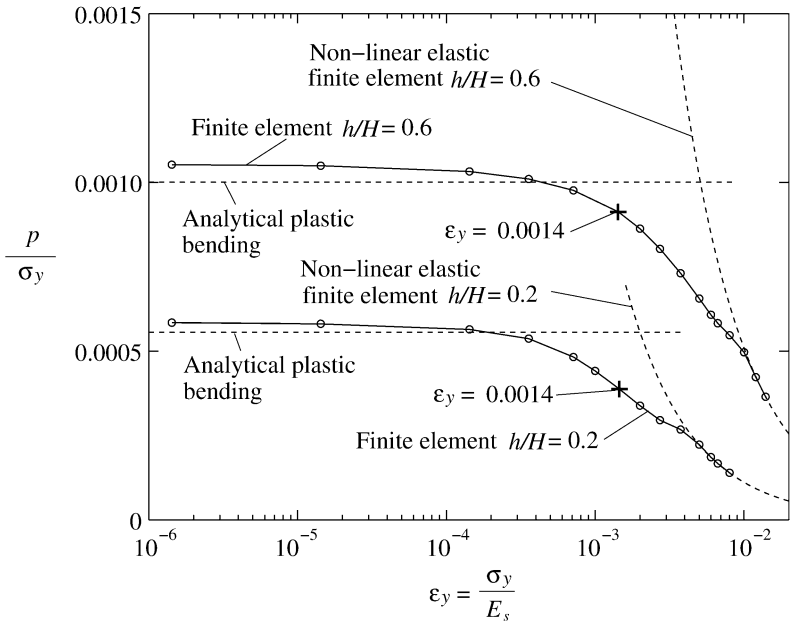

Fig. 15. The normalised peak strength p/σ_y of regular Y-cores ($\alpha = 45°$, $\bar{t} = 0.01$, $\bar{e} = 0.2$) with the no-sliding boundary condition as a function of the yield strain ϵ_y of the parent material. Results are shown for two choices of the leg height $\bar{h}$.

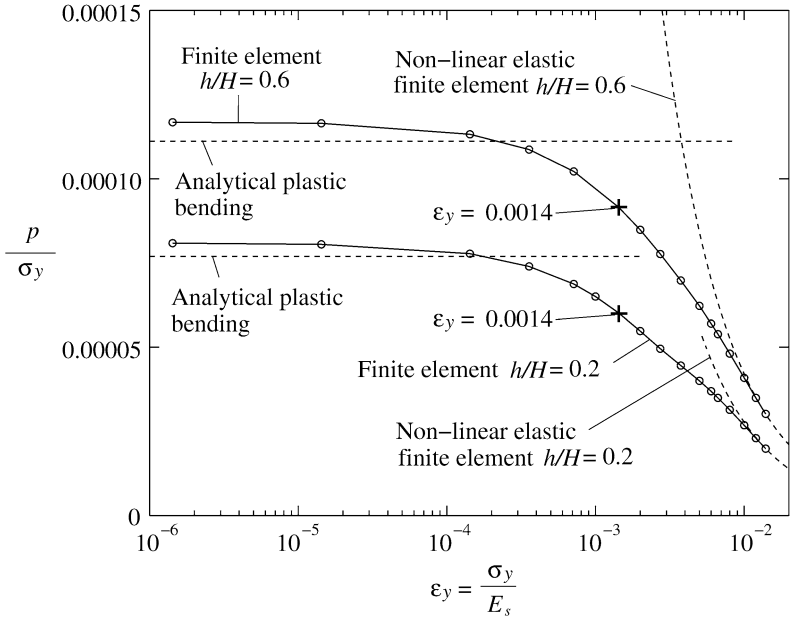

Fig. 16. The normalised peak strength p/σ_y of regular Y-cores ($\alpha = 45°$, $\bar{t} = 0.01$, $\bar{e} = 1.0$) with the no-sliding boundary condition as a function of the yield strain ϵ_y of the parent material. Results are shown for two choices of the leg height $\bar{h}$.

Finally, it is worth noting that the web of the Y-core can be thought of as an geometrical imperfection introduced into the web-less design. Thus, the buckling strength of the practical Y-cores designs with $e > 0$ is reasonably insensitive to other geometrical imperfections that might be introduced in the manufacturing process.

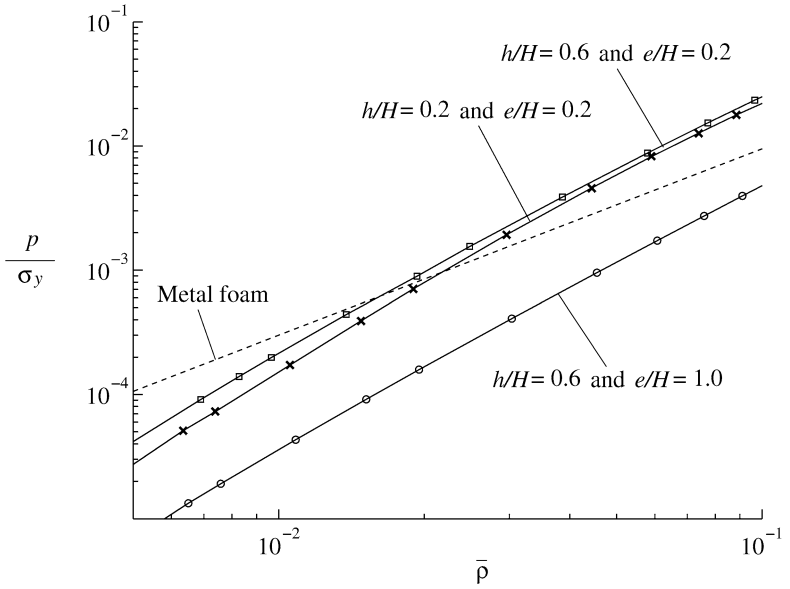

Fig. 17. Comparison of the normalised peak strength p/σ_y of three different Y-cores and metal foams. The density of the Y-cores is varied by changing $\bar{t}$.

5. Comparison with metal foams

A structural analogy exists between the Y-core and metal foams: the strength of metal foams is governed by the bending strength of the constituent struts that make-up the cellular structure. It is thus instructive to compare the strengths of the Y-core and metal foams.

Finite element predictions of the variation of the peak compressive strength of Y-cores with relative density $\bar{\rho}$ are shown in Fig. 17 for the choice $\epsilon_y = 0.0014$. The strengths of three Y-core geometries considered in this study are plotted in Fig. 17 with $\bar{\rho}$ varied by changing the sheet thickness $\bar{t}$. While reducing $\bar{h}$ from 0.6 to 0.2 is seen to have only a small effect upon the peak strength, a reduction of the web size from $\bar{e} = 1.0$ to 0.2 increases the strength of the Y-core by about an order of magnitude. Fig. 17 includes an estimate of the compressive strength of the metal foam given by Ashby et al. (2000)

$$\frac{\sigma_{\text{foam}}}{\sigma_y} = 0.3\bar{\rho}^{1.5}. \tag{15}$$

Over the range $0.005 \leqslant \bar{\rho} \leqslant 0.1$, the strength of the Y-cores with $\bar{e} = 0.2$ is comparable to metal foams. On the other hand, Y-cores having a large web ($\bar{e} = 1.0$) are substantially weaker. Note that while the strength of the three-dimensional metal foam scales as $\bar{\rho}^{3/2}$, the strength of the two-dimensional Y-core scales approximately as $\bar{\rho}^2$ in line with the plastic bending collapse mode of the regular Y-core, see Gibson and Ashby (1997) for a discussion on the scaling of the strength of cellular materials.

6. Concluding remarks

The compressive response of the web-less Y-core is stretching governed, and consequently the stiffness, elastic buckling strength and plastic collapse strength are high. However, the web-less core collapses with a steeply dropping effective stress versus strain curve, and is thereby inefficient in energy absorption. In contrast, the introduction of a web in the regular Y-core leads to a bending response. The regular Y-core is thereby much more compliant and weaker, but is more efficient in energy absorption with a flatter collapse response. The lower peak strength reduces the likelihood of shear-off in applications such as ship collisions. The compressive response of regular Y-cores made from structural alloys is in the transition regime between elastic buckling to plastic collapse. Consequently, the strength is sensitive to the assumed yield strain, and simple analytical calculations are inadequate to predict the response accurately.

It is clear that the regular Y-core has application to crash mitigation in ship structures due to its moderate transverse strength and high longitudinal strength. Recent calculations by Deshpande and Fleck (2005) suggest that it is also a suitable choice for under-water shock protection due to its ability to produce strong fluid-structure interaction effects; see Deshpande and Fleck (2005) for a full discussion.

Acknowledgements

Support from ONR (contract N00014-03-1-0283), from the NIMR on *The optimal design of Y-core sandwich structures* and from the European Union RTN project *Deformation and Fracture Instabilities in Novel materials and processes* are gratefully acknowledged.

References

Ashby, M.F., Evans, A.G., Fleck, N.A., Gibson, L.J., Hutchinson, J.W., Wadley, H.N.G., 2000. Metal Foams: A Design Guide. Butterworth–Heinemann.

Deshpande, V.S., Ashby, M.F., Fleck, N.A., 2001. Foam topology: bending versus stretching dominated architectures. Acta Mater. 49, 1035–1040.

Deshpande, V.S., Fleck, N.A., 2005. One-dimensional shock response of sandwich plates, J. Mech. Phys. Solids, submitted for publication.

Gibson, L.J., Ashby, M.F., 1997. Cellular Solids: Structure and Properties, second ed. Cambridge University Press.

Pedersen, C.B.W., 2004. Crashworthiness design of transient frame structures using topology optimization. Comput. Methods Appl. Mech. Engrg. 193 (6–8).

Rubino, V., Deshpande, V.S., Fleck, N.A., 2005. An experimental investigation of the mechanical properties of the Y-shaped sandwich core, Int. J. Mech. Sci., submitted for publication.

Timoshenko, S.P., Gere, J.M., 1963. Theory of Elastic Stability, second ed. McGraw-Hill.

Wadley, H.N.G., Fleck, N.A., Evans, A.G., 2004. Fabrication and structural performance of periodic cellular metal sandwich structures. Composite Sci. Technol. 63 (16), 2331.